Article ID: 1006-8775(2019) 02-0180-12

CAPABILITIES AND LIMITATIONS OF GRAPES SIMULATIONS OF EXTREME PRECIPITATION IN THE WARM SECTOR OVER A COMPLEX OROGRAPHY

ZHONG Shui-xin (钟水新)[1], YANG Shuai (杨 帅)[2], GUO Chun-ya (郭春伢)[3], CHEN Zi-tong (陈子通)[1]
(1. Guangdong Province Key Laboratory of Regional Numerical Weather Prediction, Institute of Tropical and Marine Meteorology, CMA, Guangzhou 510080 China; 2. Laboratory of Cloud-Precipitation Physics and Severe Storms, Institute of Atmospheric Physics Chinese Academy of Sciences, Beijing 100029 China;
3. Guangdong Meteorological Observatory, CMA, Guangzhou 510080 China)

Abstract: A comprehensive observational study on a warm sector torrential rain (WSTR) on 20 May 2016 over south China is presented with a pioneering examination of simulation capabilities based on the Global/Regional Assimilation and Prediction System for Tropical Mesoscale Model (GRAPES_TMM). The results show that the meso-scale convective boundary formed between north wind from mountainous areas and the south wind from plain regions as well as the cold outflows boundary both contribute to the convections over Xinyi, and the convections were blocked and stayed stagnant in the trumpet-shaped topography for about 8 hours which eventually caused the torrential rains. Comparative verifications of the observational studies by simulations showed that GRAPES_TMM had better estimations of large-scale frontal precipitation than the local warm-sector torrential rains. The simulations of local torrential rains in the warm sector showed strong biases in precipitation location and amount. GRAPES_TMM also showed overestimated surface winds and a faster moving speed bias, as well as an overall underestimation of the nocturnal surface temperature during the WSTR. This work may lead to several prospective researches of its model improvements on model physics such as land surface process and PBL parameterization.

Key words: warm sector torrential rain (WSTR); trumpet-shaped topography; GRAPES_TMM; mesoscale convective boundary
CLC number: P458 **Document code:** A
doi: 10.16555/j.1006-8775.2019.02.005

1 INTRODUCTION

Warm Sector Torrential Rains (WSTRs) are one of the most influential weather systems during the flood seasons over the south of China. They could not only cause severe damages by the destructive flood, but also are very difficult to predict. WSTRs may bring a sudden extreme rainfall either in the mountainous region or in an urban area over this part of China without any apparent early synoptic signals, which could lead to poor performance of routine operational forecasts and numerical simulations. WSTRs usually occur in a warm zone either with a surface front in the north or even without a front over the south of China. Observation experiments in the late 1970s confirmed that WSTRs account for the primary torrential rains during the flood season over southern China (Huang[1]). Owing to the comprehensive influences of the Westerlies and tropical weather systems as well as the dynamic and thermodynamic impacts of the complex underlying surface, WSTRs cause difficulties in daily operational forecasts during the flood seasons in the south of China.

To study the formation of WSTRs over the south of China, Zhong and Chen emphasized the influences of a low-level jet (LLJ) in the planetary boundary layer (PBL)[2]. Wu and Luo found that the southward movement of a cold outflow boundary may exert a profound influence on continuous convection initiation [3]. Other local environmental factors also have huge impacts on the formation of the WSTR such as topographic effects, distribution of the land and sea (Tao[4]), easterly reflux and strong southwest monsoon burst (Lin[5]). The warm sector of extratropical cyclones in the United States, compared to the torrential rains caused in the warm sector over China, are likely to contribute to other extreme weather such as severe convective storms and tornado outbreaks (e.g., Fujita et al.[6]; Galway[7]; Hamill et al.[8]). In the warm sector, warm and moist air carried by strong low-level southerly winds and upper-level cold and dry air brought

Received 2018-05-09; **Revised** 2019-03-14; **Accepted** 2019-05-15
Foundation item: National Natural Science Foundation of China (41505084); Guangzhou Science and Technology Project (201804020038); Guangdong Province Public Welfare Research and Capacity Construction Project (2017B020218003); China Meteorological Administration Special Public Welfare Research Fund (GYHY201406003); Guangdong Meteorological Service Project (2015B01)
Biography: ZHONG Shui-xin, Ph. D., associate researcher, primarily undertaking research on mesoscale dynamics and analysis.
Corresponding author: YANG Shuai, e-mail: ys_ys@126.com

by the strong westerly winds provide an environment favorable for severe convective storms (e.g., Hamill et al.[8]; Johns and Doswell[9]; Tochimoto and Niino[10]). Warm sector tornadoes are associated with a stronger, negatively tilted synoptic storm system as well as additional thermodynamic and kinematic parameters pertaining to low-level moisture and environmental winds (Boustead et al.[11]) without discernible surface boundaries (Corfidi et al. [12]). In addition, storm relative environmental helicity and convective available potential energy are notably strong in the warm sector for outbreak cyclones[10]. Moreover, the 300-hPa jet exit region and downstream of increasing absolute vorticity in the warm sector may contribute to significant tornadoes.

The generation of convection by the impacts of a boundary has received considerable research concern (Maddox et al. [13]; Atkins et al. [14]; Davis and Lee [15]). Experiments results showed that the area from 10 km on the warm side to 30 km on the cool side of the boundary was a favorable region for tornado development (Rasmussen et al.[16]). Srock and Bosart suggested that the cool pool formed near the mountain slopes was partially blocked by the higher terrain, and the coastal front on the oceanward edge of the cool pool was likely to become a focusing mechanism for ascent and precipitation [17]. Carbone et al. showed that the organization and propagation of those rainbands were influenced by a low-level cold pool and the pressure gradient that resulted from a blocked flow[18]. Wu and Luo found that the boundary in the warm sector was formed between a cold dome generated by previous Meso-scale Convective System (MCS)-generated cold outflow and higher equivalent potential temperature southwesterly flow from the ocean[3]. Fritsch et al. suggested that the cold pool could be maintained by the blocking of incoming solar radiation due to cloud cover over the cold dome and evaporative cooling due to precipitation falling through the cold dome[19]. However, Schumacher and Boustead found that strong low-level mesocyclones and tornadoes could be formed and developed in an area with no discernible surface boundaries[20]. They noted that a warm sector without discernible surface boundaries was more favorable for the genesis of classic supercells, but it could only produce short-lived tornadoes. Yu and Lin found that colder nearshore air that resulted from the combined effects of orographic blocking, the evaporation of the Taiwan rainbands precipitation, and radiative cooling over coastal land could continue to persist and acted to provide a continuing source of lifting for the subsequent maintenance of moist convection[21].

In spite of the achievement in the above-mentioned diagnostic study on the WSTRs, few studies focus on the predictability of WSTRs based on numerical weather prediction (NWP). An idealized experiment conducted by Tochimoto and Niino[10] showed that the differences in the cyclone structure and environmental parameters caused by tornado outbreaks could be qualitatively explained by the dry dynamics. The sensitive experiments from the Weather Research and Forecasting (WRF) model showed that WRF could predict the distribution and intensity of the precipitation. The simulation were largely dependent on the PBL scheme[2], and the South China Sea (SCS) atmospheric moisture transportation was crucial in triggering the precipitation of the WSTRs over the south of China. This paper will examine the capabilities of Global/Regional Assimilation and Prediction System (GRAPES) for the Tropical Mesoscale Model (GRAPES_TMM) on the simulation of the WSTRs by the presence of a cold front in proper position with respect to the local terrain.

The objectives of this study are to evaluate the reliability of the GRAPES_TMM model simulations of the WSTRs focusing on complex orography over Xinyi, and to complement these observational comparisons with an examination of meteorological observations. Questions that motivate the study include the following:

(1) What are the performances of the GRAPES_TMM model on the simulation of the WSTR and the corresponding environmental characteristics?

(2) What are the characteristics of the WSTRs by which specific orographic distribution affects heavy rainfall in Xinyi?

(3) What are the limitations of GRAPES_TMM simulations of WSTRs over the complex orography over the south of China?

The paper will be organized as follows. The data used in this study is described in section 2, and the rainfall and environmental conditions are outlined in section 3. Target verification of the warm sector simulations are given in section 4, followed by a conclusion and discussion in section 5.

2 DATA AND METHODOLOGY

2.1 *Event selection*

The extreme precipitation over the south of China on 20 May 2016 was chosen in this study. The torrential rain caused huge damages by its short-time heavy rainfall, including 5 deaths and 4 missing and more than 1 billion *yuan* worth of economic losses. The maximum accumulated daily rainfall reaches 464 mm, which is the maximal daily rainfall amount recorded by the surface rain gauges over the mainland of China during the annually first rainy season of 2016. The heaviest rainfall is located around Xinyi City, which is characterized by a trumpet-shaped topography over the west of Guangdong Province (Fig. 1). The north of Xinyi is dominated by the Shuang Jiding Mountain (SJ, 1,227m) and the northwest is dominated by the Liu Wuding Mountain (LW, 1,337m), as well as northern and western steep ridges of the Yun Kai Mountain (YK, 1,704m) and the south is the city of Mao Ming (MM) covered by low valleys and areas of flat terrain. Fig. 2 shows the temporal evolution of hourly surface wind and rainfall amount from two stations over the Xinyi area. It can be seen that the heavy rainfall

period was mainly concentrated during 0200-0800 UTC 20 May and the major peak appearing 0300-0400 UTC 20 May. It also can be seen that the temperature and winds had significant diurnal variations, which shows that the rainfall was occurring at the cooling stage of the stations with some interesting wind variations during the rainfall.

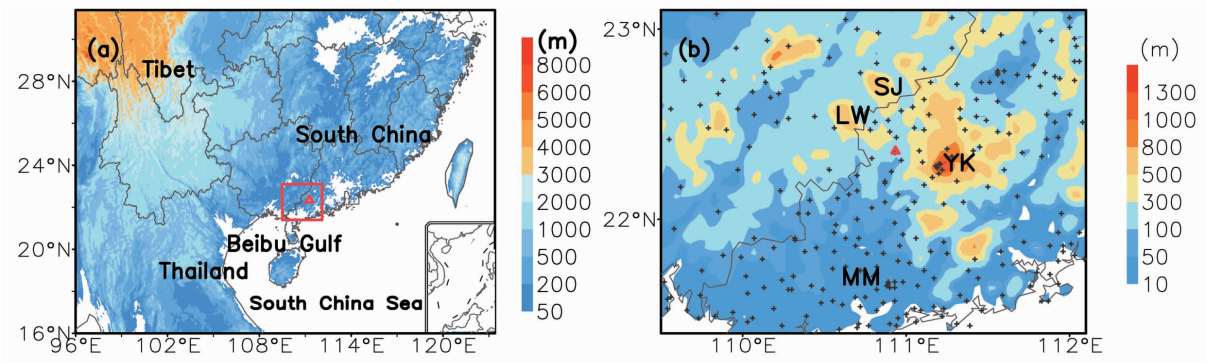

Figure 1. (a) Domain of MARS (3 km). Color shading denotes the orography, and the red frame shows the area of concern in (b). (b) The 24-h accumulated precipitation (contour, mm), location of the surface observations and the zoomed orography (shaded) of Xinyi, the red triangle denotes the location of Xinyi, where the torrential rain occurred.

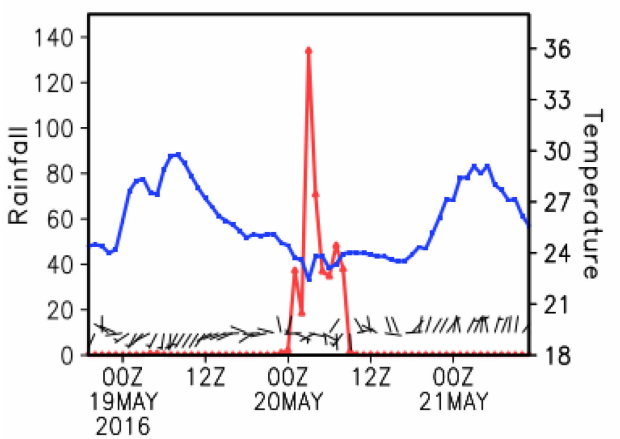

Figure 2. Time series of average hourly surface temperature (blue line, ℃), winds (bars) and precipitation by Xinyi and an adjacent station (G2539).

2.2 *Model description*

The model used in this study is the new-generation Mesoscale Atmospheric Regional Model System (MARS) in operation over the south of China based on GRAPES_TMM (Zhong et al. [22]). MARS focuses on short-range forecasting of mesoscale convective systems over this part of China. The physics package used in this paper is the same as that used in Zhong and Chen[23], but without the convective cumulus scheme. The simulation domain comprises 913×513 grid points, with a horizontal resolution of 3 km, as shown in Fig. 1a. There are 60 layers in the vertical direction, and both the initial and lateral boundary fields are obtained from the 0.125° × 0.125° forecast field of the European Centre for Medium-Range Weather Forecasts (ECMWF), with the lateral boundary field updated every 6 h.

2.3 *Verification datasets*

The large scale environmental characteristics are analyzed by using the ECMWF Reanalysis (ERA-Interim, Dee et al. [24]) that provides 6-hourly interval grid point values (0000, 0600, 1200, and 1800 UTC) with a resolution of 1.25°×1.25° at 16 levels. The vertical grid spacing is 25 hPa from 1,000 to 750 hPa, and 50 hPa from 750 to 500 hPa. The elements used herein include zonal and meridional components of wind (u and v), vertical wind velocity (w), temperature (T), specific humidity (q).

The hourly radar reflectivity data and surface observations are used to analyze the MCSs evolution and climatic characteristics of the variables. The surface meteorological variables extracted from this dataset include hourly averaged wind speed, hourly maximum wind speed, wind direction, temperature and precipitation amount at 1-h intervals. Radar reflectivity was combined from the meteorological radar stations over the south of China.

3 RAINFALL AND ENVIRONMENTAL CONDITIONS

The extreme rainfall event of interest occurred in the west coastal area of Guangdong Province. Fig. 3 shows the environmental conditions at 925 hPa during this extreme rainfall event. It can be seen that there was a high potential pseudo-equivalent temperature tongue (θ_{se}, >351 K) stretched into the southwest and the south of China from the Beibu Gulf (BG) and SCS, accompanied by a trough extending northeastward from the southeast of YG Plateau. At 1800 UTC 19 May, the high θ_{se} tongue and the trough were located in the midwest of Guangxi, which provided a favorable environment for large-scale convective systems over these regions. By 0000 UTC 20 May, the trough, characterized by a convergence center and a strong horizontal gradient of θ_{se}, was located in the north central part of Guangxi, and the west of Guangdong was located in front of the trough.

It can be seen that from Fig. 4 that MARS captured the general large-scale synoptic pattern over the south of China, including the northward stretching high θ_{se} tongue and the trough, especially for the distribution and

intensity of the high θ_{se} tongue during the occurrence of the WSTRs at 0000 UTC 20 May. Nevertheless, the simulated θ_{se} over the south of Guangdong was stronger than in the ERA interim reanalysis. It can be seen that the high θ_{se} at 351K was stretching much more northward than in the reanalysis at 1800 UTC 19 May. In addition, the θ_{se} over the north of Guangxi was stronger than in the reanalysis at 2000 UTC 20 May. Both reanalysis and simulation show that there were strong horizontal gradient of θ_{se} behind the trough over the north of Guangxi.

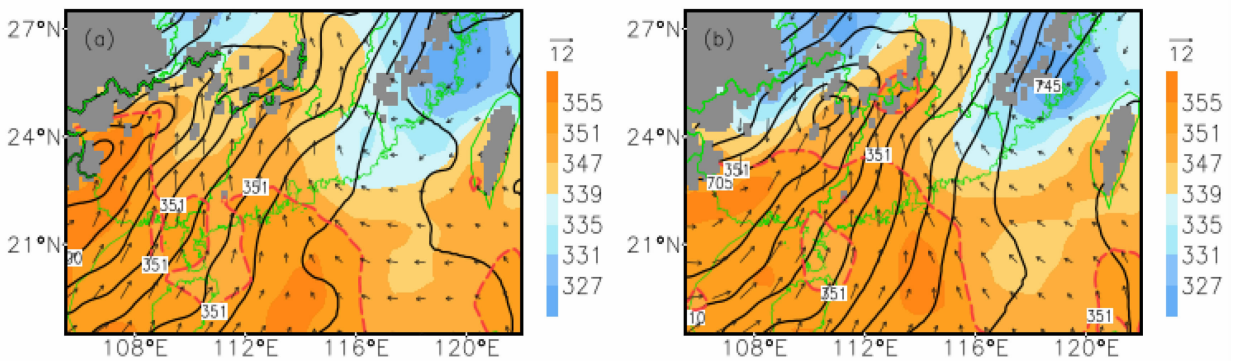

Figure 3. Potential pseudo-equivalent temperature (shaded, unit: K), horizontal wind, and geopotential height at 925 hPa (contours, 10 gpm) of the ERA interim analysis data at (a) 1800 UTC May 19 and (b) 0000 UTC May 20, 2016; the gray shade indicates topography.

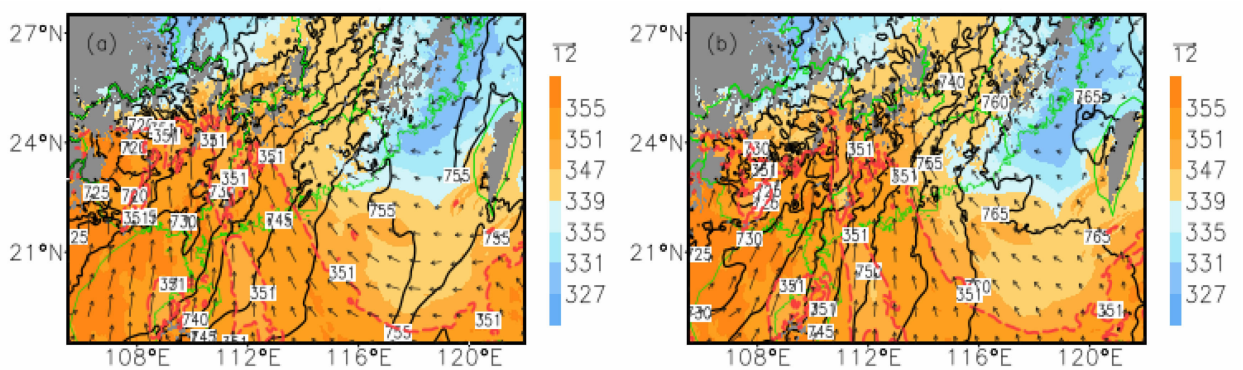

Figure 4. As in Fig. 3, but for the simulation.

To further diagnose the processes contributing to the development of trough and to analyze its environmental impacts, the frontogenesis was calculated as this high thermal gradient may associate with a front (e.g., Sanders[25]). The frontogenesis (Hoskins[26]), defined as the Lagrangian rate of change of the magnitude of the horizontal potential temperature(θ_{se}) gradient in this study.

$$F=\frac{\mathrm{d}}{\mathrm{d}t}|\nabla_p\theta_{se}|, \tag{1}$$

$$\frac{\partial}{\partial t}+u\frac{\partial}{\partial x}+v\frac{\partial}{\partial y}+w\frac{\partial}{\partial p} \tag{2}$$

$$\nabla_p=i\frac{\partial}{\partial x}+j\frac{\partial}{\partial y} \tag{3}$$

where F denotes the frontogenesis function, t is the time variation, x, y and p represent meridian, zonal and vertical variation

Figure 5 shows the frontogenesis distribution 0000 UTC 20 May at 925 hPa. It can be seen that a frontogenesis function was mainly located in the middle of Guangxi, and the simulation of the front was consistent with the reanalysis. Xinyi was located in front of the front without large scale cold air interactions to these regions. Researches on the warm-sector in the United States show that the convections in parts of the Great Plains in the warm sector were not present in the enhanced frontogenesis[11]. Moreover, unlike the tornadoes occurring in the warm-sector in this region, the environmental conditions of WSTRs over the south of China did not show typical environmental characteristics at 300 hPa (e. g., the exit region of a 300-hPa jet maximum), which suggest that the lower troposphere may have great impacts on the formation of the WSTRs. Fig. 6 gives the comparison between observations and simulations of the 24-h accumulated precipitation by 1200 UTC 20 May. It can be seen that the simulated frontal precipitation by MARS showed a good agreement with the observation. In contrast, MARS showed a significant underestimation of the precipitation over Xinyi. The simulated 24-h accumulated precipitation over Xinyi was about 50 mm, while the observation reached 464 mm at Xinyi. In the meantime, MARS missed the torrential rains over coastal regions and north of Guangdong, and the underestimation of the precipitation over mountains exists in most of the NWP models (e.g., Colle et al. [27]; Alcott and

Steenburgh[28]; McMillen and Steenburgh[29]). It can be inferred that MARS generally produced realistic total precipitation distributions in terms of large-scale environmental systems. While the simulations of torrential rains in the warm sector showed strong biases in precipitation location and amount. These biases were located over the corresponding complex terrain in Guangdong (Fig. 1), especially over YK Mountains in Xinyi.

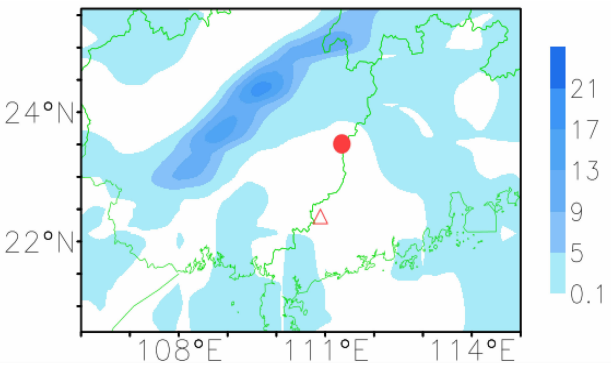

Figure 5. Distribution of frontogenesis (shaded, unit: 10^{-9}K·s^{-1}) at 950 hPa by 0000 UTC May 20, 2016. The red triangle denotes the location of Xinyi and the red dot denotes the sounding location of Wuzhou.

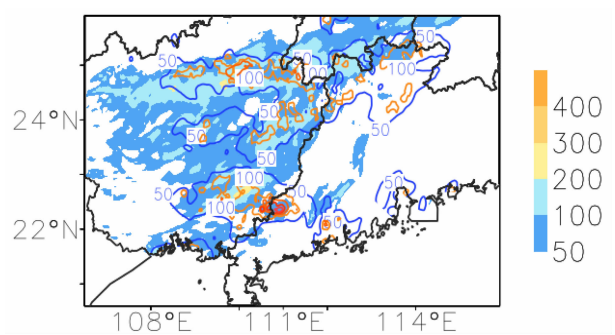

Figure 6. Comparison of 24-h accumulated precipitation between observation (contour) and simulation (shaded, unit: mm) at 1200 UTC May 20, 2016.

4 TARGET VERIFICATION OF THE WARM SECTOR SIMULATIONS

4.1 *PBL verification*

The performances on the simulation of PBL winds by MARS are examined using the ERA-Interim data and sounding of Wuzhou. It can be seen that there was an increasing wind at 925 hPa along the trough from 1800 UTC 19 to 0000 UTC 20 May (Fig. 7). The strong south wind in front of the trough formed a LLJ at the strongest stage with the maximum wind speed larger than 14 m·s^{-1} at 0000 UTC 20 May, and the LLJ was weakened since 0000 UTC 20 May. Xinyi was located in front of the LLJ with the wind speed between 8 m·s^{-1}and 10 m·s^{-1} by 0000 UTC 20 May. The extreme precipitation occurred within 8 hours during the southward moving of the LLJ from 0000 UTC 20 May (as shown in Fig. 2).The simulations show that MARS basically captured the evolutions of the winds. However, the winds over Xinyi were overestimated by 0000 UTC 20 May (Fig. 8), which was about 2 m·s^{-1} larger than the reanalysis. Moreover, the moving speed of the simulated trough was also a little faster than the reanalysis. For example, the simulated trough reached the east of Guangxi, while the reanalysis showed that the trough was located in the mideast of Guangxi. The fast moving speed of the systems is a longtime phenomenon existing in the high resolution operational forecasting systems of GRAPES_TMM and other NWP models (e.g., Met Office, Cotton et al.[30]).

The nearest sounding by Wuzhou and the vertical section along Xinyi were analyzed to examine the performance of MARS on winds simulation at different levels. It can be seen that the simulation of the wind profile showed a good agreement with the observations (Fig. 9), including the wind speed and directions at different levels. The cross-section comparison shows that MARS successfully captured the warm environment and unstable layers over Xinyi (Fig. 10). Nevertheless, there was an underestimated wind in the north of Xinyi and an overestimation over Xinyi. The results are consistent as that shown in Fig. 7.

4.2 *Surface diagnosis and verification*

Surface observations are used to diagnose the characteristics of WSTRs and to further examine the corresponding performance of MARS. It can be seen that the surface observations had experienced significant diurnal changes before the occurrence of the WSTR. For example, the surface temperature over the mountainous region experienced a dramatic decrease by about 4 ℃ from more than 27 ℃ at the nightfall to less than 24 ℃ at the middle night with a corresponding local wind change from south wind to north wind (Fig. 11). Nocturnal cooling may have contributed to the observed surface temperature and winds changes. In the meantime, the weak southeast wind over the plain region increased to a stronger south wind, which thus provided a favorable convective environment by surface convergence from the north wind in the mountainous region and the south wind over the plain region.

However, the simulation by MARS failed to reproduce the evolutional characteristics of surface temperature and winds. The model showed an overall underestimation of the nocturnal surface temperature during the WSTRs, especially over the plain region in the midnight (at 1900 UTC 19 May, Fig. 12). The surface temperature over the mountainous region was higher than 27 ℃ by 1200 UTC 19 May, while the simulated temperature was about 24 ℃, which was about 3 ℃ lower than the observation. Furthermore, MARS failed to capture the north wind over the mountainous regions and showed an overall overestimation of south wind over these regions. The surface wind speed was about 3 m·s^{-1} in the plain region, while simulated southeast wind reached more than 5 m·s^{-1}.

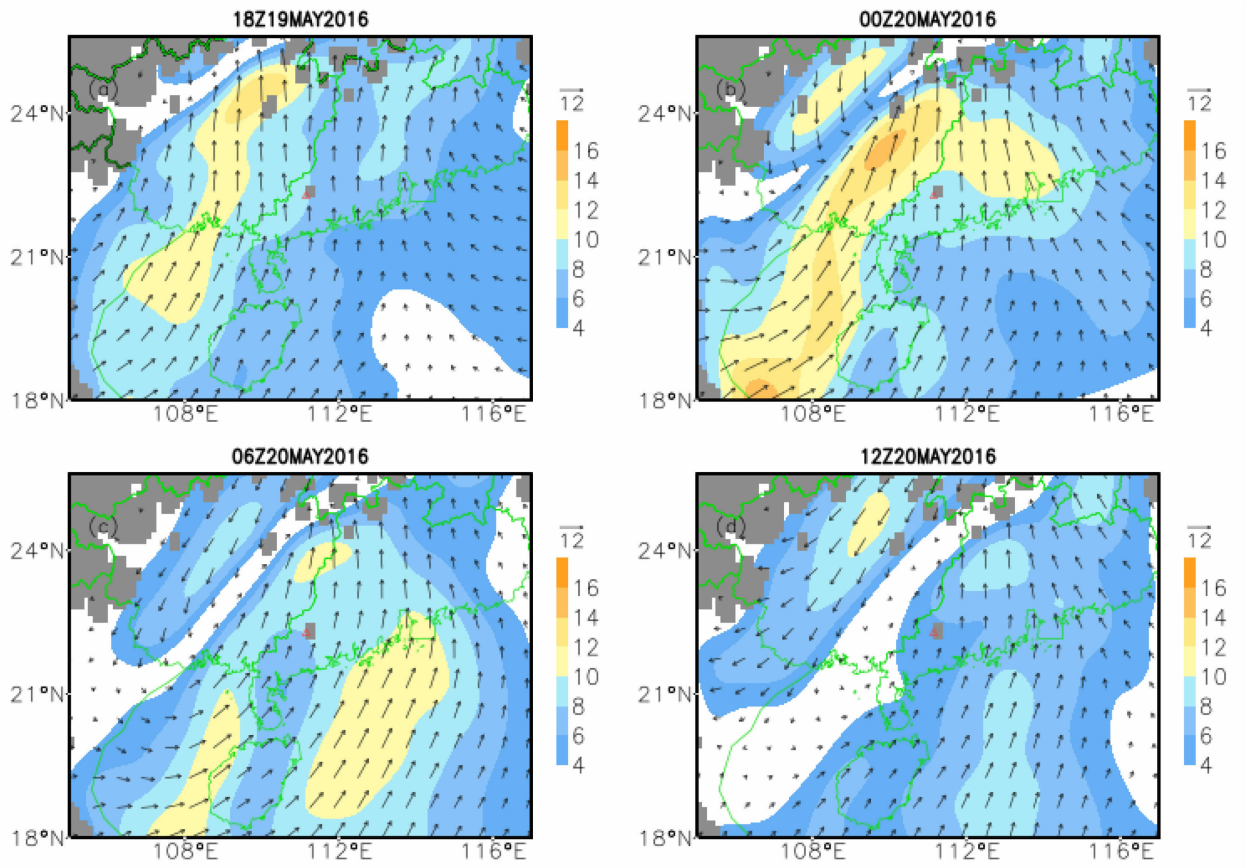

Figure 7. The wind vectors and wind speed (shaded, $m \cdot s^{-1}$) at 925 hPa from ERA interim analysis data at (a) 1800 UTC May 19; (b) 0000; (c) 0600; (d) 1200 UTC May 20, 2016; the gray shade indicates topography.

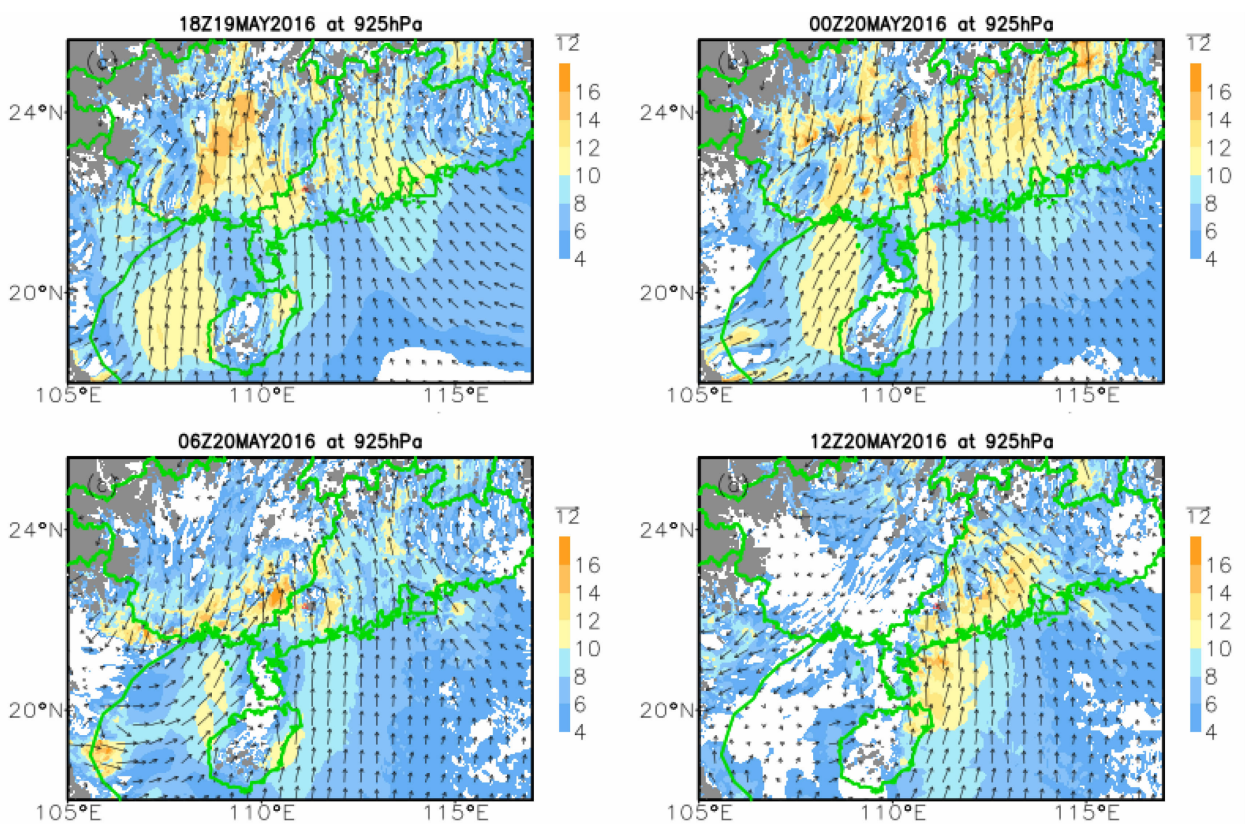

Figure 8. As in Fig. 7, but for the simulation.

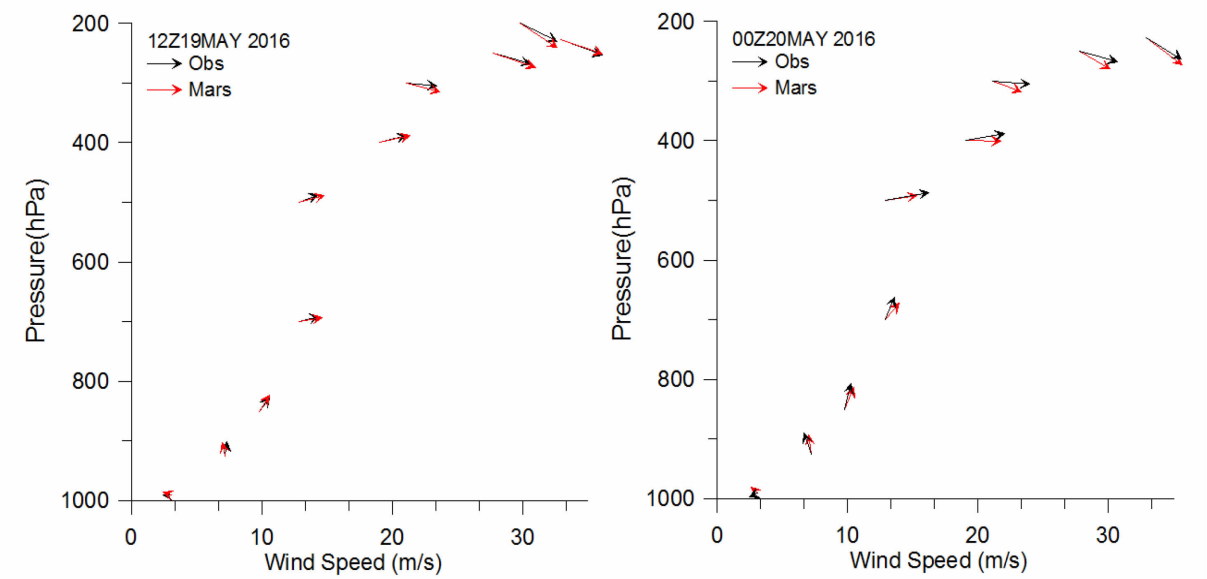

Figure 9. The horizontal winds by Wuzhou sounding, the red vectors represent simulation and the black vectors are observations. (a) 1200 UTC May 19; (b) 0000 UTC May 20, 2016.

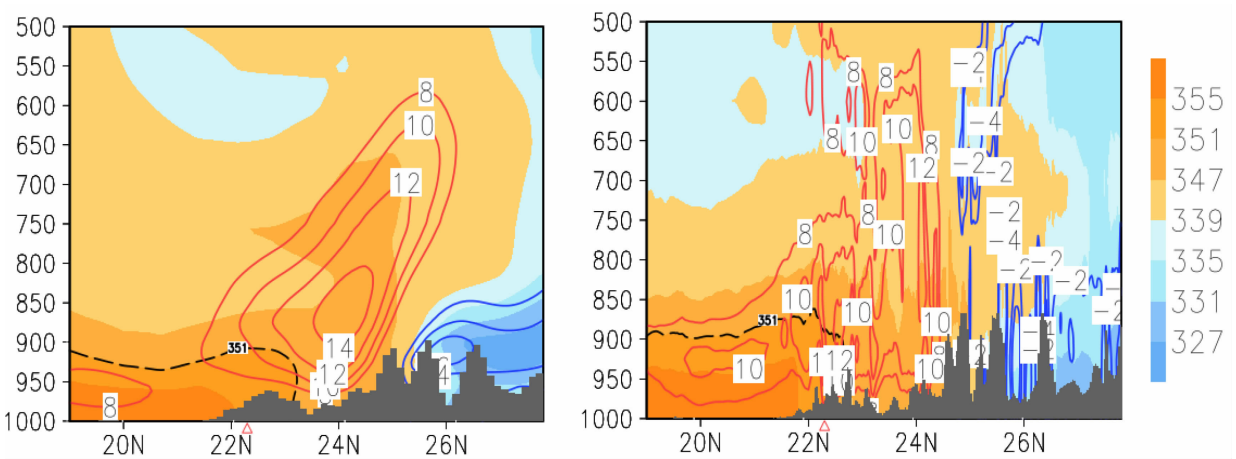

Figure 10. Vertical section of potential pseudo-equivalent temperature (shaded, unit: K, the thick dashed line shows the value of 351 K), vertical flow and geopotential height along 111°E at 0000 UTC on May 20, 2016; the grey shade indicates topography. (a) ERA interim analysis; (b) simulation. The red triangles at the abscissa indicate the location of Xinyi.

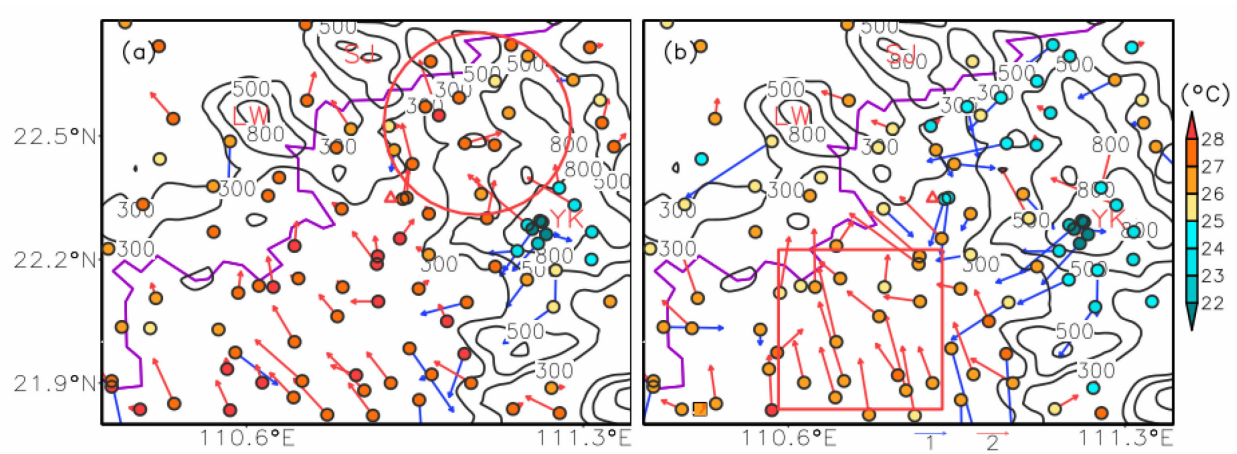

Figure 11. Surface temperature (dots) and winds observations (m·s^{-1}, the red vector denotes the south wind, the blue vector represents north wind) at (a) 1200; (b) 1900 UTC May 19, 2016; the black contours indicate topography. The red circle in (a) represents the mountainous observations and the red rectangle denotes the plain area.

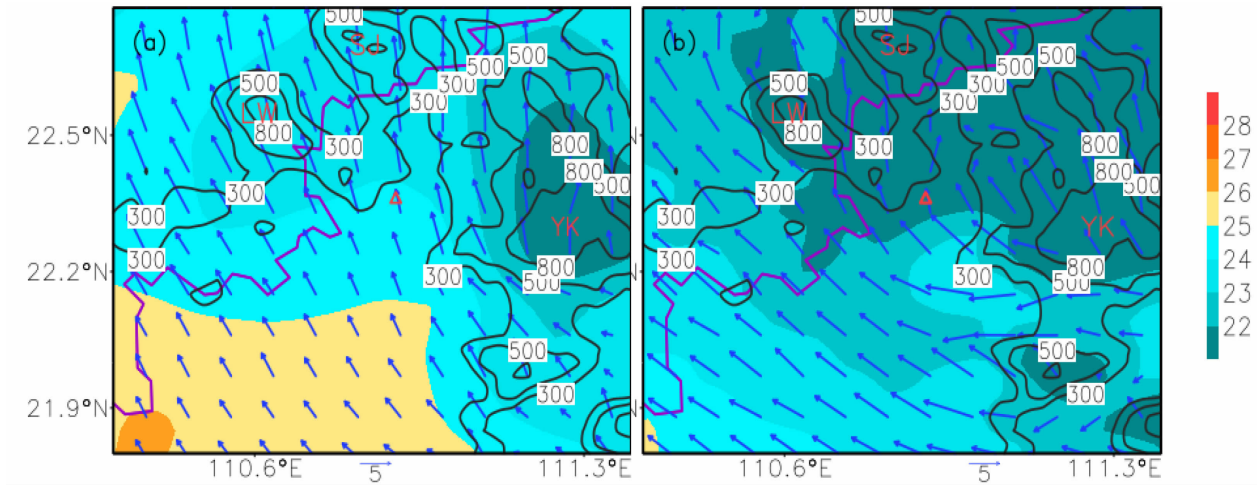

Figure 12. As in Fig. 11, but for the simulation.

To further examine changes in surface observations and corresponding model performance, radar variables and MARS variables are also analyzed for a larger region in Fig. 13. The surface wind showed a similar distribution (see Fig. 11b), with increasing south wind in the plain regions and north wind over the mountainous regions. It can be seen that new MCSs with the radar reflectivity stronger than 30 dBZ generated over the south of LW Mountain by 2200 UTC May 19 (Fig. 13), which might be caused by the lifting effects of the mountain, and the convections showed an eastward shifting trend towards Xinyi. Furthermore, new convections generated in the southeast of SJ Mountain and merged with the eastward moving MCS from the south of LW Mountain, which contributed to a continuously increasing intensity of the convections. Besides, the convergence between south

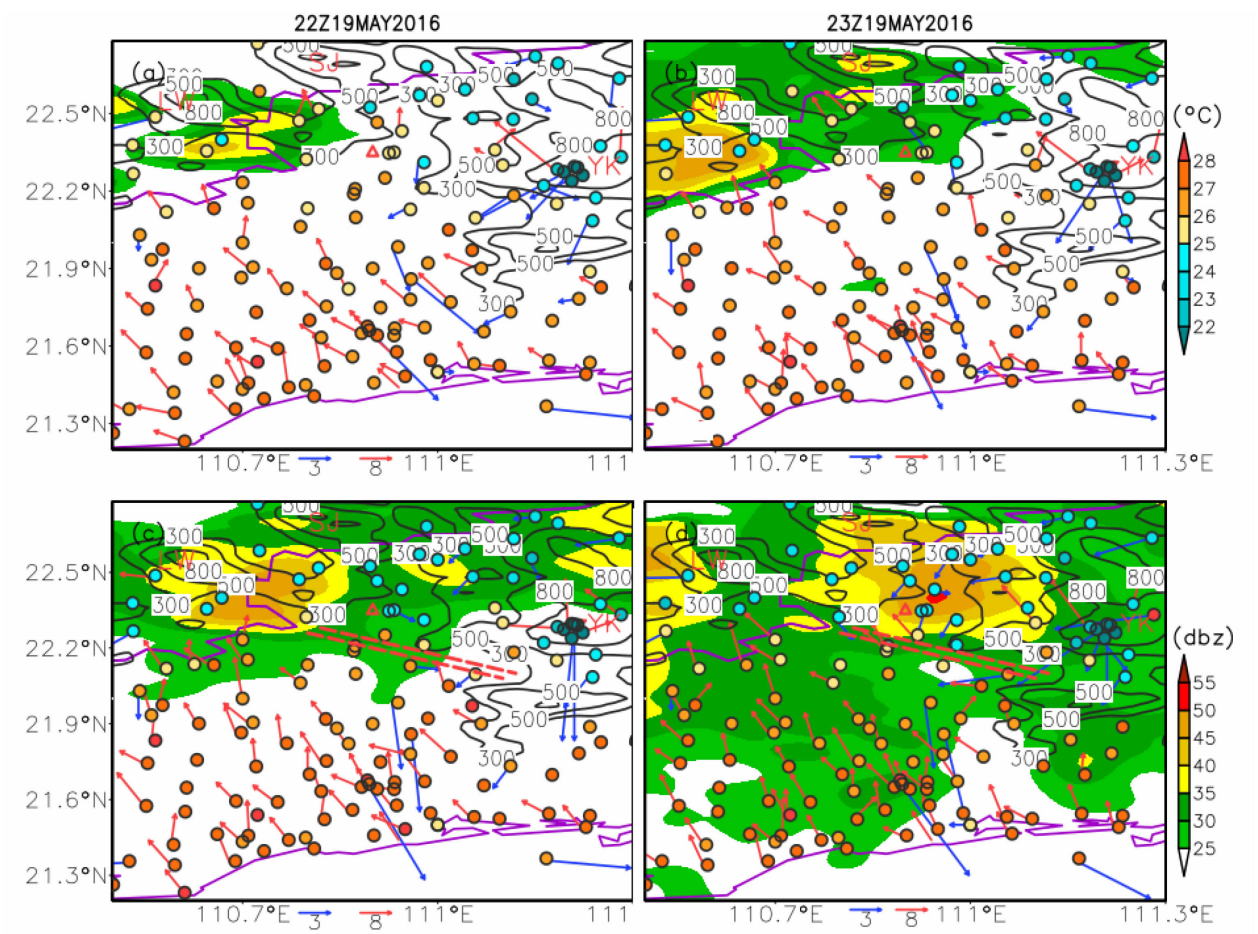

Figure 13. Surface temperature (dots) and winds observations ($m \cdot s^{-1}$, the red vector denotes the south wind, the blue vector represents the north wind) at (a) 2200; (b) 2300 UTC May 19; (c) 0000; (d) 0100 UTC May 20, 2016; the black contours denote topography and the colored shades represent radar reflectivity; the double red contours denote the meso-scale convective boundary.

winds from plain regions and north winds from mountainous areas triggered a meso-scale convective boundary (MCB) over Xinyi. Due to the combined effects, the convections over Xinyi grew rapidly and reached a strong stage within 3 hours, and the center convections were stronger than 50 dBZ by 0100 UTC May 20. Thus, both the north winds caused by the east-ward moving effects of the MCS and the strengthened south wind had great impacts on the formations of the MCB. On the other hand, the cold outflows from the MCB strengthened the intensity of the convections, and the maintenance and the strengthening of the MCB caused the torrential rains over Xinyi.

Between 2300 UTC May 19 and 0000 UTC May 20 in the morning, the surface temperature over the plain regions showed a small increase of about 1 ℃ due to the solar radiation effects. It should be noted that the surface temperature showed an overall warm environment over the plain regions. Substantial differences of surface temperature are evident between observations and simulations (Fig. 14). It can be seen that MARS showed a generally cold bias between 2200 UTC and 2300 UTC, especially over the plain regions. Nevertheless, MARS showed a rapid increase of surface temperature between 0000 UTC and 0100 UTC in the morning. At 0200 UTC, the coverage of the convections extended to most of the trumpet-shaped topography over Xinyi (Fig. 15). By 0300-0400 UTC, the intensity reached the mature stage with the radar reflectivity stronger than 50 dBZ over east of YK Mountain. It also can be seen that some strong cold outflows were triggered and the south winds were strengthened, especially by 0300-0400 UTC. The strong cold outflows might contribute to the further strengthening of the convections. Then these convections were blocked and stayed stagnant in the trumpet-shaped topography over Xinyi about 8 hours from 0000-0900 UTC. Unlike the nocturnal cold bias of surface temperature and overestimation of surface winds, MARS showed a reasonable simulation on diurnal surface temperature and winds.

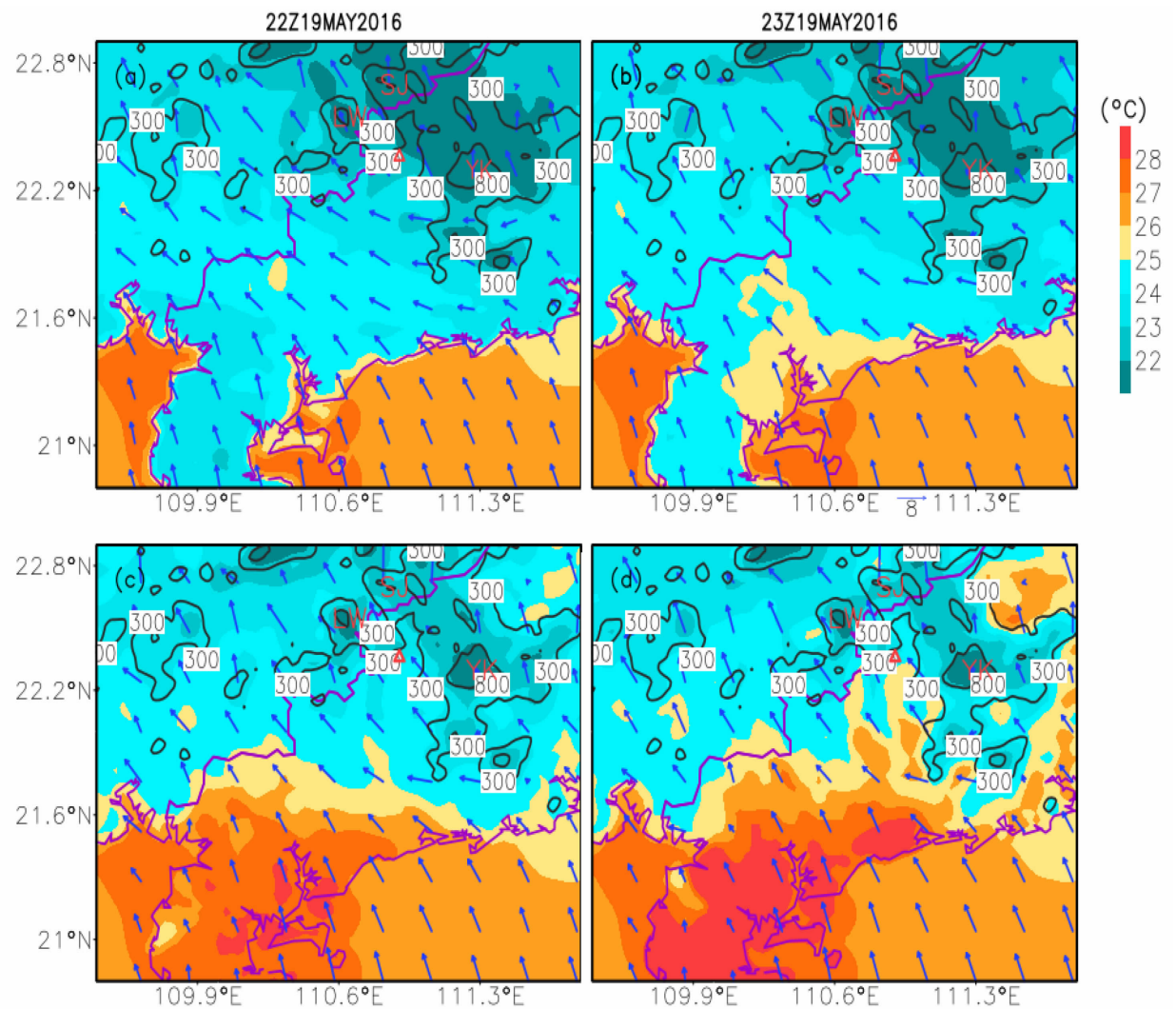

Figure 14. The simulated surface temperature (shaded) and winds ($m \cdot s^{-1}$) at (a) 2200; (b) 2300 UTC May 19; (c) 0000; (d) 0100 UTC May 20, 2016; the black contours denote topography.

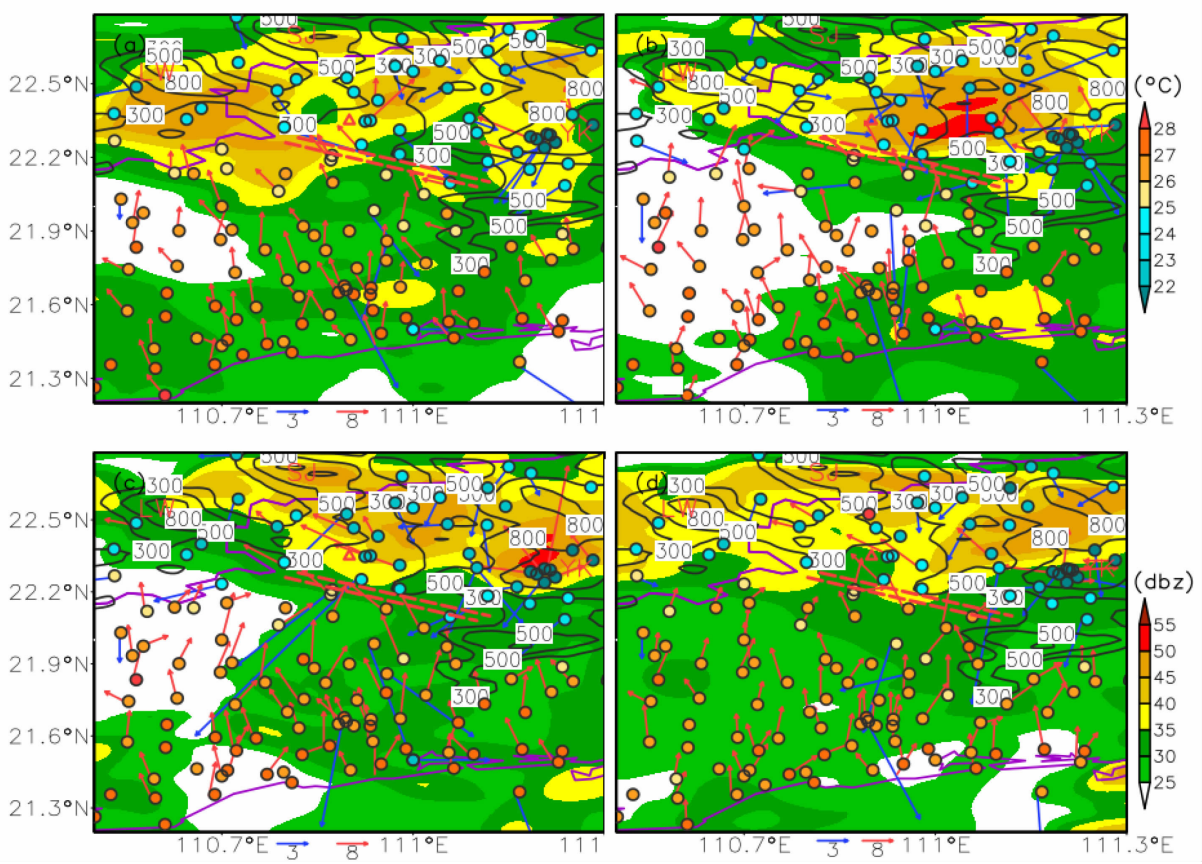

Figure 15. As in Fig. 13, but for (a) 0200; (b) 0300; (c) 0400 and (d) 0500 UTC.

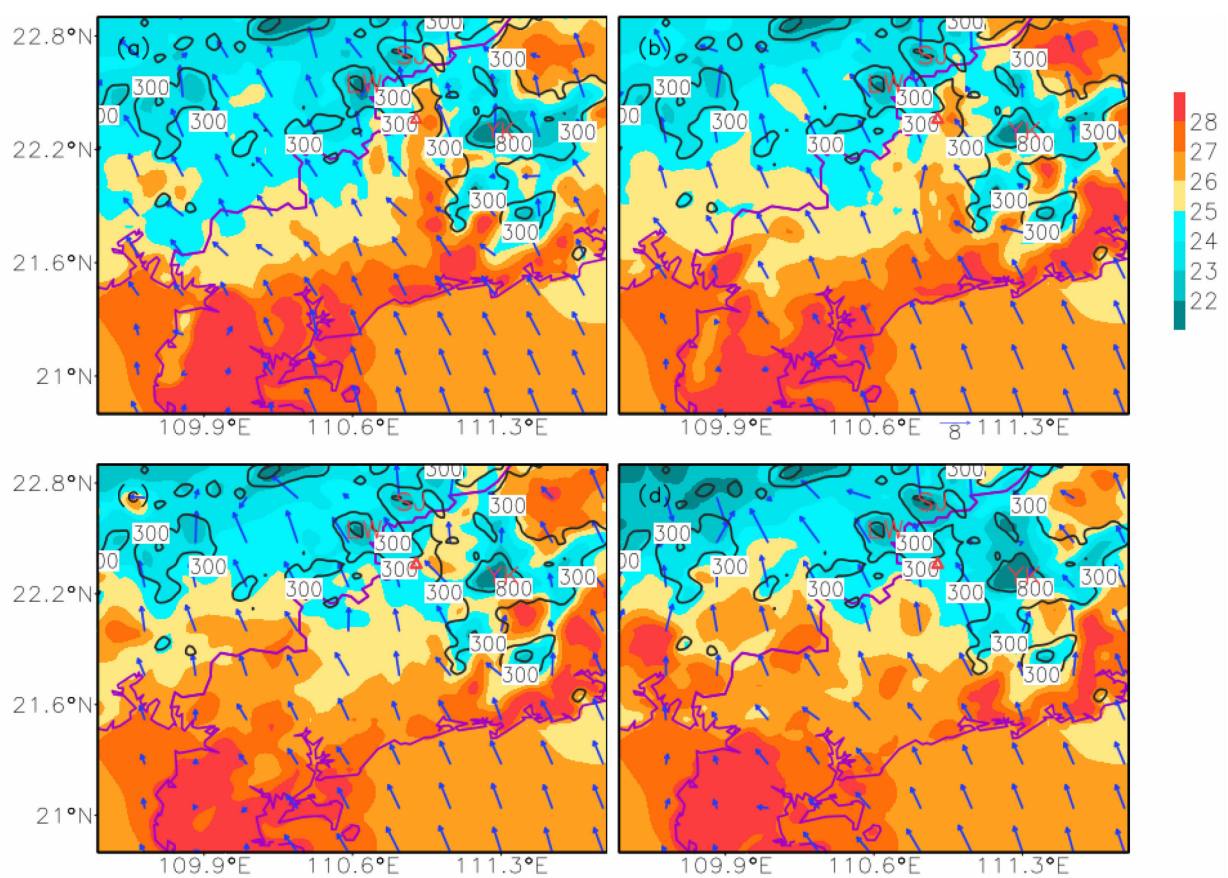

Figure 16. As in Fig. 14, but for (a) 0200; (b) 0300; (c) 0400 and (d) 0500 UTC.

5 CONCLUSIONS AND DISCUSSIONS

This study presents a comprehensive observational study on the torrential rains in the warm sector on 20 May 2016 over the south of China, and conducts a pioneering examination of the corresponding NWP performance by the GRAPES_TMM model. The results show that both the unique topography and the southerly nocturnal surges contribute to the extreme precipitation. Comparative verifications of the observational studies by simulations showed that GRAPES_TMM had better estimations of large-scale frontal precipitation than the local warm-sector torrential rains. Though the large-scale high θ_{se} tongue in the warm sector was well captured by the model in terms of comparisons with 6-h interval ERA interim reanalysis, the simulations of local surface characteristics including temperature and winds showed some apparent biases by using the hourly surface observations. Main findings are summarized as follows:

(1) The WSTR was triggered in the trumpet-shaped topography over Xinyi, accompanied with a high potential pseudo-equivalent temperature tongue that stretched into Xinyi and with an upstream trough that extended northeastward from the southeast of YG Plateau. The simulations showed that GRAPES_TMM could simulate the general large-scale synoptic pattern over the south of China, including the northward stretching high θ_{se} tongue and the trough in Guangxi, as well as the large-scale frontal precipitation, while the simulations of local torrential rains in the warm sector showed strong biases in precipitation location and amount.

(2) The extreme precipitation occurred in the MCB that formed between the north wind from mountainous areas and the south wind from plain regions during the southward moving of the LLJ which was located in front of the trough. Though the simulations show that the model basically captured the evolutions of the LLJ, the winds over Xinyi were overestimated and thus the MCB was missed during the occurrence of the WSTR, accompanied with a faster moving speed bias than the reanalysis, which suggests that the rapid evolution of the systems is a long-standing problem in GRAPES_TMM.

(3) The model showed an overall underestimation of the nocturnal surface temperature about 3 ℃ and thus failed to predict the temperature differences between the mountainous areas and plain regions during the WSTR. Observational analysis showed that cold outflows caused by the MCB might further contribute to the enhancement of the convergence with the increasing south wind, and the convections were blocked and stayed stagnant in the trumpet-shaped topography for about 8 hours over Xinyi, which eventually caused the torrential rains due to all factors mentioned above.

It should be noted that an accurate evaluation of its performance on WSTRs simulations is not possible due to the lack of high resolution observational data. In particular, the ECMWF reanalysis, though representing well for large-scale synoptic conditions, still has its limitation in reflecting the meso-scale and convective scale systems. In spite of that, this work is the first systematic assessment based on the diagnostic study of WSTRs over the south of China by using GRAPES_TMM. The related results could lead to the exploration of several prospective researches of its model improvements on model physics such as land surface process and PBL parameterization in the future.

REFERENCES:

[1] HUANG Shi-song. The Pre-flood Season Rains Southern China[M]. Guangzhou: Guangdong Science and Technology Press, 1986, 1-244 (in Chinese).

[2] ZHONG Shui-xin, CHEN Zi-tong. The impacts of atmospheric moisture transportation on warm sector torrential rains over south China [J]. Atmos, 2017, 8(7): 116.

[3] WU Meng-wen, LUO Ya-li. Mesoscale observational analysis of lifting mechanism of a warm-sector convective system producing the maximal daily precipitation in China mainland during pre-summer rainy season of 2015[J]. J Meteor Res, 2016, 30(5): 719-736.

[4] TAO Shi-yan. The Chinese Rainstorms [M]. Beijing: Chinese Science Press, 1980, 1-225 (in Chinese).

[5] LIN Liang-xun. Guangdong Weather Forecast Technical Manual [M]. Beijing: China Meteorological Press, 2006: 1-526 (in Chinese).

[6] FUJITA T, BRADBURY D L, Van THULLENAR C F. Palm Sunday tornadoes of April 11, 1965[J]. Mon Wea Rev, 1970, 98(1): 29-69.

[7] GALWAY J G. Some climatological aspects of tornado outbreaks [J]. Mon Wea Rev, 1997, 105(4): 477-484.

[8] HAMILL T M, SCHNEIDER R S, BROOKS H E, et al. The May 2003 extended tornado outbreak[J]. Bull Amer Meteor Soc, 2005, 86(4): 531-542.

[9] JOHNS R H, DOSWELL C A. Severe local storms forecasting [J]. Wea Forecasting, 1992: 588-612.

[10] TOCHIMOTO E, NIINO H. Structural and environmental characteristics of extratropical cyclones that cause tornado outbreaks in the warm sector: A composite study [J]. Mon Wea Rev, 2016, 144(3): 945-969.

[11] BOUSTEAD J M, MAYES B E, GARGAN W, et al. Discriminating environmental conditions for significant warm sector and boundary tornadoes in parts of the Great Plains [J]. Wea Forecasting, 2013, 28(6): 1498-1523.

[12] CORFIDI S, WEISS S, KAIN J, et al. Revisiting the 3-4 April 1974 super outbreak of tornadoes[J]. Wea Forecasting, 2010, 25(2): 465-510.

[13] MADDOX R A, HOXIT L R, CHAPPELL C F. A study of tornadic thunderstorm interactions with thermal boundaries [J]. Mon Wea Rev, 1980, 108(3): 322-336.

[14] ATKINS N T, WEISMAN M L, WICKER L J. The influence of preexisting boundaries on supercell evolution [J]. Mon Wea Rev, 1999, 127(12): 2910-2927.

[15] DAVIS C A, LEE W C. Mesoscale analysis of heavy rainfall episodes from SoWMEX/TiMREX[J]. J Atmos Sci, 2012, 69(2): 521-537.

[16] RASMUSSEN E N, STRAKA J M, DAVIES-JONES R, et al. Verification of the origins of rotation in tornadoes experiment: VORTEX [J]. Bull Amer Meteor Soc, 1994,

75(6): 995-1006.
[17] SROCK A F, BOSART L F. Heavy precipitation associated with southern Appalachian cold-air damming and Carolina coastal frontogenesis in advance of weak landfalling Tropical Storm Marco (1990) [J]. Mon Wea Rev, 2009, 137(8): 2448-2470.
[18] CARBONE R E, COOPER W A, LEE W C. Forcing of flow reversal along the windward slopes of Hawaii [J]. Mon Wea Rev, 1995, 123(12): 3466-3480.
[19] FRITSCH J M, KAPOLKA J, HIRSCHBERG P A, et al. The effects of subcloud-layer diabatic processes on cold air damming [J]. J Atmos Sci, 1992, 49(1): 49-70.
[20] SCHUMACHER P N, BOUSTEAD J M. Mesocyclone evolution associated with varying shear profiles during the 24 June 2003 tornado outbreak [J]. Wea Forecasting, 2011, 26(6): 808-827.
[21] YU C K, LIN C Y. Formation and maintenance of a long-lived Taiwan rainband during 1-3 March 2003 [J]. J Atmos Sci, 2017, 74(4): 1211-1232.
[22] ZHONG Shui-xin, CHEN Zi-tong, WANG Gang. Improved forecasting of cold air outbreaks over southern China through orographic gravity wave drag parameterization[J]. J Trop Meteor, 2016, 22(4): 522-534.
[23] ZHONG Shui-xin, CHEN Zi-tong. Improved wind circulations and precipitation forecasts over southwest china using a modified orographic parameterization scheme [J]. J Meteor Res, 2015, 29(1): 132-143
[24] DEE D P, UPPALA S M, SIMMONS A J, et al. The ERA- Interim reanalysis: Configuration and performance of the data assimilation system[J]. Quart J Roy Meteor Soc, 2011, 137(656): 553-597.
[25] SANDERS F. A short-lived cold front in the southwestern United States [J]. Mon Wea Rev, 1999, 127(10): 2395-2403.
[26] HOSKINS B J. The mathematical theory of frontogenesis[J]. Ann Rev Fluid Mech, 1982, 14(1): 131-151.
[27] COLLE B A, WESTRICK K J, MASS C F. Evaluation of MM5 and Eta-10 precipitation forecasts over the Pacific Northwest during the cool season[J]. Wea Forecasting, 1999, 14(2): 137-154.
[28] ALCOTT T I, STEENBURGH W J. Orographic influences on a Great Salt Lake- effect snowstorm [J]. Mon Wea Rev, 2013, 141(7): 2432-2450.
[29] McMILLEN J D, STEENBURGH W J. Capabilities and limitations of convection-permitting WRF simulations of lake-effect systems over the Great Salt Lake[J]. Wea Forecasting, 2015, 30(6): 1711-1731.
[30] COTTON J, FORSYTHE M, SAUNDERS R, et al. AMVs at the Met Office: Activities to improve their impact in NWP[C]// 11th International Winds Workshop, Auckland, 2012: 1-33.

Citation: ZHONG Shui-xin, YANG Shuai, GUO Chun-ya, et al. Capabilities and limitations of GRAPES simulations of extreme precipitation in the warm sector over a complex orography [J]. J Trop Meteor, 2019, 25(2): 180-191.